Supporting Information for

Article

CO_2 Hydrogenation to Methane over Ni-Catalysts; the Effect of Support and Vanadia Promoting

Izabela S.Pieta [1,*]Agnieszka Lewalska-Graczyk [1], Pawel Kowalik [2], Katarzyna Antoniak-Jurak [2], Mikolaj Krysa [3], Anna Sroka-Bartnicka [3,4], Arkadiusz Gajek [1], Wojciech Lisowski [1], Dusan Mrdenovic [1], Piotr Pieta [1], Robert Nowakowski [1], Agata Lew [5] and Ewa M. Serwicka [6]

[1] Institute of Physical Chemistry Polish Academy of Science, 01-224 Warsaw, Poland; alewalska-graczyk@ichf.edu.pl (A. L.-G.); agajek@ichf.edu.pl (A.G.); wlisowski@ichf.edu.pl (W.L.), dmrdenovic@ichf.edu.pl (D. M.); ppieta@ichf.edu.pl (P. P.); rnowakowski@ichf.edu.pl (R. N.); ipieta@ichf.edu.pl (I.S.P.);

[2] Łukasiewicz Research Network - New Chemical Syntheses Institute, 24-110 Pulawy, Poland; pawel.kowalik@ins.lukasiewicz.gov.pl (P.K.); katarzyna.antoniak@ins.lukasiewicz.gov.pl (K.A.J.);

[3] Department of Biopharmacy, Medical University of Lublin, Chodzki 4a, 20-093 Lublin, Poland; mikolaj.krysa@gmail.com (M.K.); anna.sroka@umlub.pl (A.S.B.);

[4] Department of Genetics and Microbiology, Maria Curie-Skłodowska University, Akademicka 19, 20-033 Lublin, Poland; anna.sroka-bartnicka@umlub.pl (A.S.B.);

[5] Chemeko - System SP. z o.o, 54-519 Wroclaw, Poland; agata.lew@chemekosystem.pl (A. L.);

[6] Jerzy Haber Institute of Catalysis and Surface Chemistry PAS, Niezapominajek 8, 30239 Krakow, Poland; ncserwic@cyf-kr.edu.pl (E. S.);

* Correspondence: ipieta@ichf.edu.pl; Tel.: +48-223-432-092 (I. S. P.)

Table S1. Catalyst screening in CO_2 methanation.

No.	Catalyst	Preparation method	CO_2 conversion, %	CH_4 selectivity, %	T, K	Ni content, wt%	H_2/CO_2 ratio	GHSV, h^{-1}	Ref.
1	Ni/γ-Al_2O_3	wet impregnation	82	100	623	20	4/1	9000	3–82
2	Ni/MSN	sol-gel	85	99.9	623	5	4/1	50000	3
3	Ni/$Ce_{0.12}Zr_{0.88}$[1]	co-precipitation	97	99	523	15	19/1[2]	5000	7
4	Ni/TiO2	deposition-precipitation	96	99	533	15	4/1	2400	7
5	Ni/Al_2O_3	wet impregnation	75	100	773	14	5/1	52300	7
6	Ni/Al_2O_3	coprecipitation	100	99.7	510	25	9/1	2400	7
7	Ni/CeO_2	wet impregnation	90	100	553	20	4/1	30000	1
8	Ni/ZrO_2	wet impregnation	81	100	553	20	4/1	30000	1
9	Ni/γ-Al_2O_3–ZrO_2–TiO_2–CeO_2	wet impregnation	81	100	573	16.5	4/1	20000	7[1]
10	Ni/Y_2O_3	wet impregnation	78[3]	>98[3]	623	10	4/1	20000	2
11	Ni/Al_2O_3	wet impregnation	76[3]	>98[3]	623	10	4/1	20000	2
12	Ni/ZrO_2	wet impregnation	76[3]	>98[3]	623	10	4/1	20000	2
13	Ni/CeO_2	wet impregnation	73[3]	>98[3]	623	10	4/1	20000	2
14	Ni/Sm_2O_3	wet impregnation	68[3]	>99[3]	573	10	4/1	20000	2
15	JM57-4Q	na.	100	72	623	24	4/1	6700	88
16	NiWP	co-precipitation	90	>97	623	7	5/1	12000	this work
17	NiR	wet impregnation	43	>63	623	17	5/1	12000	this work
18	NiVR	wet impregnation	67	>90	623	17	5/1	12000	this work

[1] NH_3 treated
[2] coke gas
[3] calculated from published data
*Commercial methane steam reforming catalyst from Johnson Matthey

88 . *Garbarino, G.; Kowalik, P.; Riani, P.; Antoniak-Jurak, K.; Pieta, P.; Lewalska-Graczyk, A.; Lisowski W.; Nowakowski, R.; Busca, G.; S.Pieta, I.; Improvement of Ni/Al2O3 catalysts for low-temperature CO2 methanation by vanadium and calcium oxide addition. Ind. Eng. Chem. Res. ACS, 2021, accepted.*

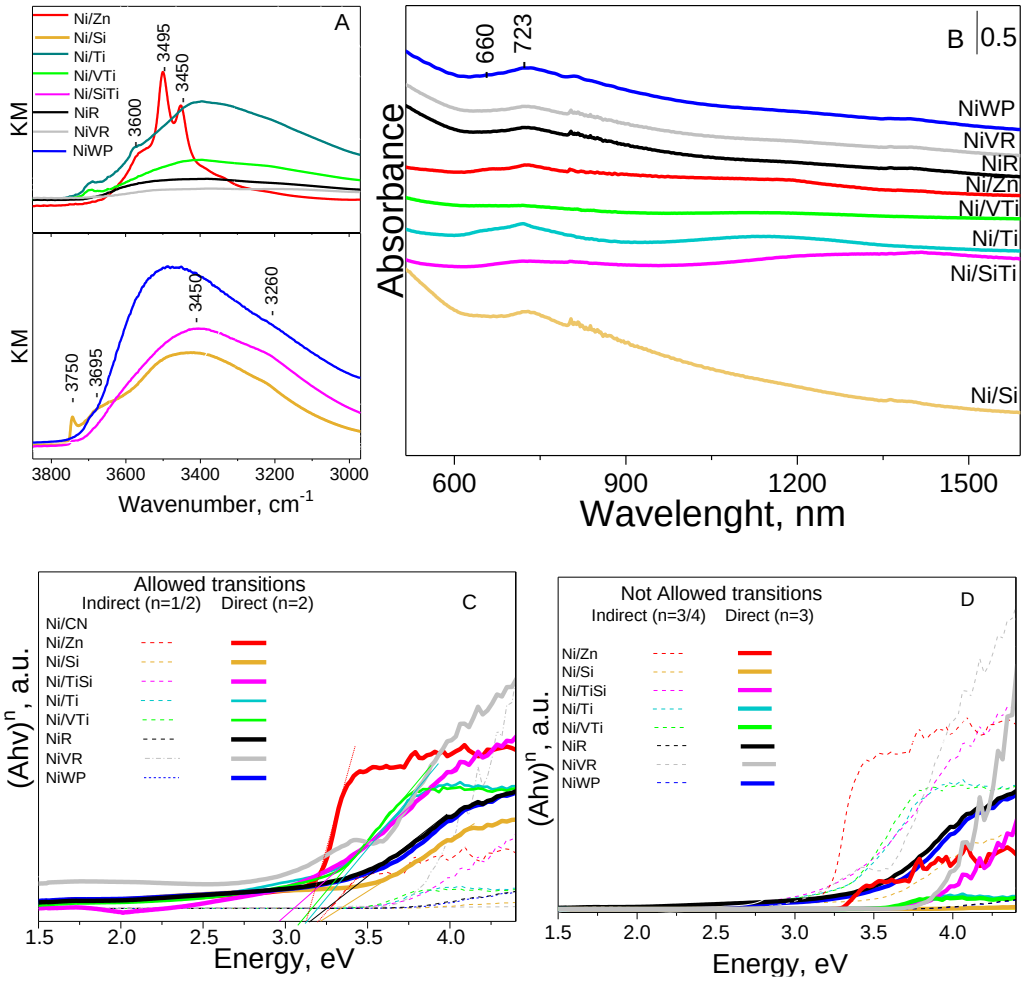

Figure S1. DRIFT spectra of Ni-supported catalysts, A) whole range spectra B) enhanced OH-re-gion. UV-VIS spectra (A, B) and Tauc plots for allowed (C) and not allowed transitions (D) for Ni-supported catalysts.

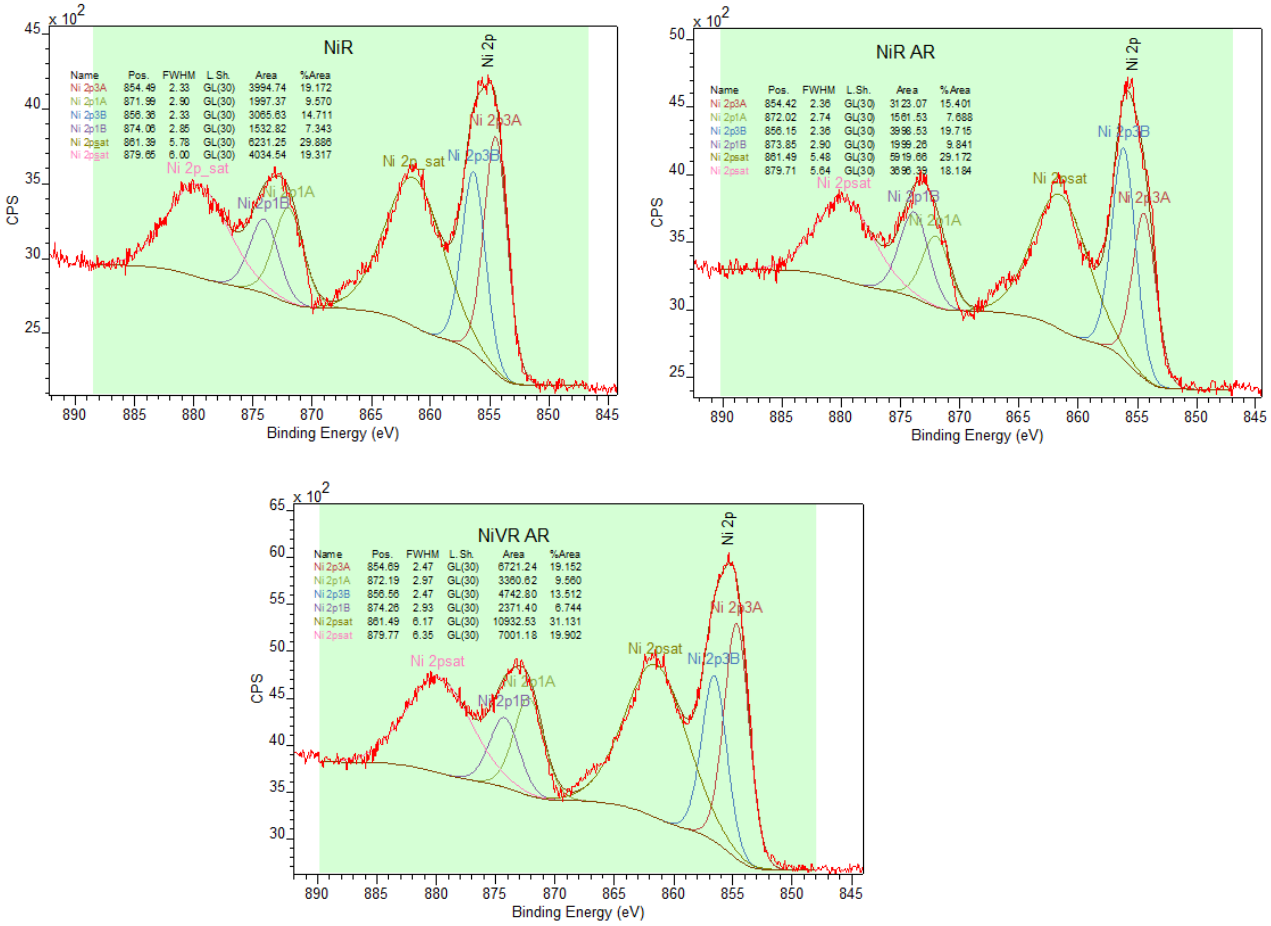

Figure S2. High resolution and deconvoluted spectra of Ni2p peak.

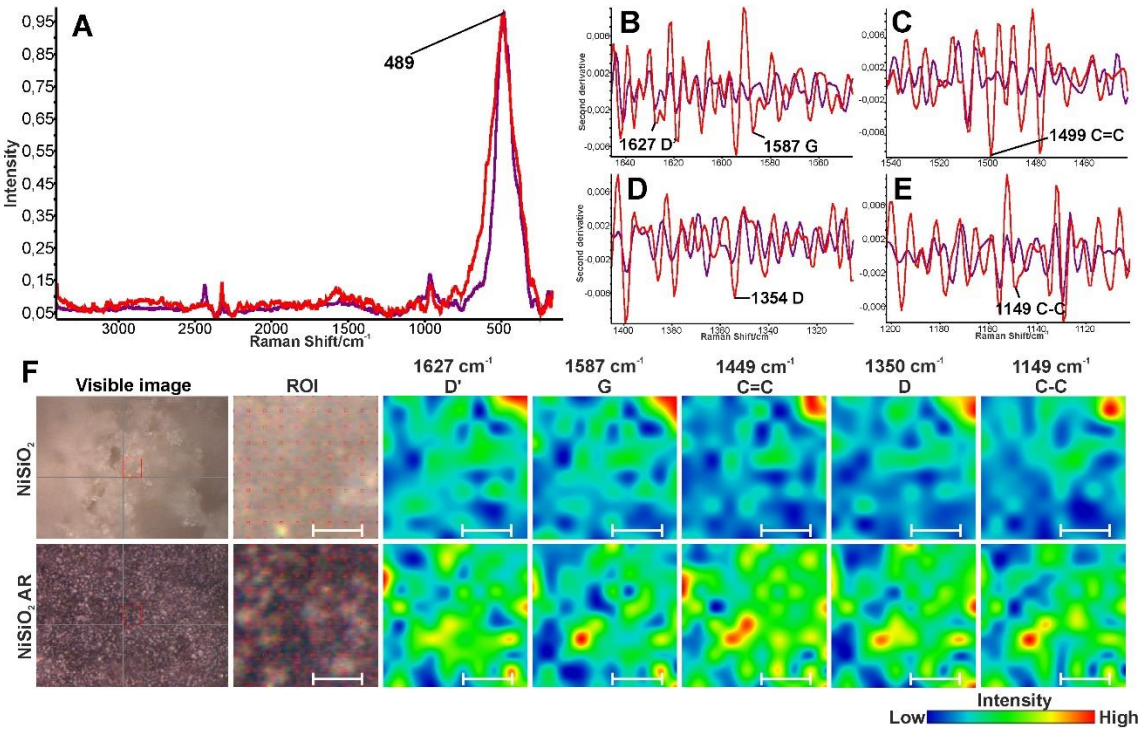

Figure S3. Raman spectra and chemical maps of the $NiSiO_2$ before and after reaction (AR). The red spectrum corresponds to the AR sample; the violet spectrum corresponds to the sample before reaction. A) Normalized spectra to the highest band B) Second derivative spectra of the region 1646–1546 cm^{-1} C) Second derivative spectra of the region 1542–1442 cm^{-1} D) Second derivative spectra of the region 1405–1305 cm^{-1} E) Second derivative spectra of the region 1202–1102 cm^{-1} F) Raman maps with distribution of selected bands for $NiSiO_2$ and $NiSiO_2$ AR. The white scale bar corresponds to 4,5 µm.

The Raman spectra of $NiSiO_2$ before and after reaction (AR) are presented in Fig. S3, with most intense bands at 478 cm^{-1}. This band can be assigned to O-Si-O and Si-O-Si bending vibration,[2] and is wider for $NiSiO_2$ AR than for the $NiSiO_2$ before reaction. The broader band may be due to the polymerization of SiO_2 caused by high temperature of the reaction.[3]

[2] (a) S. Kundu, B. Satpati, T. Kar, S. Kumar Pradhan, Microstructure characterization of hydrothermally synthesized PANI/V2O5·nH2O heterojunction photocatalyst for visible light induced photodegradation of organic pollutants and non-absorbing colorless molecules J. Hazardous Mat., 339 (2017) 161-173.
(b) G. Socrates, Infrared and Raman characteristic group frequencies, ISBN: 978-0-470-09307-8, (2001).
(c) P. Tarte, Infrared spectra of inorganic alumi-nates and characteristic vibrational frequencies of AIO4 tetrahedra and A106 octahedra. , Spectrochem. Acta 23 A (1967) 2127-2143.
(d) M.J. Lázaro, Y. Echegoyen, I. Suelves, J.M. Palacios, R. Moliner, Decomposition of methane over Ni-SiO2 and Ni-Cu-SiO2 catalysts: Effect of catalyst preparation method, Appl. Catal. A: General, 329 (2007) 22-29.
(e) Y. Xie, J. You, L. Lu, M. Wang, J. Wang, Raman Spectroscopic Study of Coal Samplesduring Heating, Appl. Sci., 9 (2019) 4699

[3] (a) S. Kundu, B. Satpati, T. Kar, S. Kumar Pradhan, Microstructure characterization of hydrothermally synthesized PANI/V2O5·nH2O heterojunction photocatalyst for visible light induced photodegradation of organic pollutants and non-absorbing colorless molecules J. Hazardous Mat., 339 (2017) 161-173.
(b) G. Socrates, Infrared and Raman characteristic group frequencies, ISBN: 978-0-470-09307-8, (2001).
(c) P. Tarte, Infrared spectra of inorganic alumi-nates and characteristic vibrational frequencies of AIO4 tetrahedra and A106 octahedra. , Spectrochem. Acta 23 A (1967) 2127-2143.

The second derivative spectra presented in the Figure S3 B, C, D, E shows significant changes in the chemical composition. Both of the spectra contain the D' band at 1627 cm^{-1} corresponding to in-plane carbon–carbon stretching normal vibrations of imperfect or disordered graphite in the sample. The bands at 1354 cm^{-1} and 1587 cm^{-1}, characteristic of disordered graphite (D band) and highly crystalline graphite (G band), respectively, were detected. The band at 1499 cm^{-1} corresponding to C=C stretching vibration and the band at 1149 cm^{-1} corresponding to C-C stretching vibration of graphene or graphite are present.[2] They are not present in the spectrum before reaction. The spectrum after reaction shows D band at 1354 cm^{-1} corresponding to imperfect graphite.[2] This band is shifted and significantly more intensive than in $NiSiO_2$ before reaction.

The analysis of the spectra allows to postulate that the catalyst itself was not significantly changed during the performed reaction, suggesting that it is stable in the reaction conditions.

The chemical images of the Raman map show similar intensity throughout the whole map. In the sample after reaction, the presented bands have lower intensity on the white spots seen on the visible image. Moreover all of the investigated bands in the sample after reaction were distributed similarly.

(d) M.J. Lázaro, Y. Echegoyen, I. Suelves, J.M. Palacios, R. Moliner, Decomposition of methane over Ni-SiO2 and Ni-Cu-SiO2 catalysts: Effect of catalyst preparation method, Appl. Catal. A: General, 329 (2007) 22-29.
(e) Y. Xie, J. You, L. Lu, M. Wang, J. Wang, Raman Spectroscopic Study of Coal Samplesduring Heating, Appl. Sci., 9 (2019) 4699

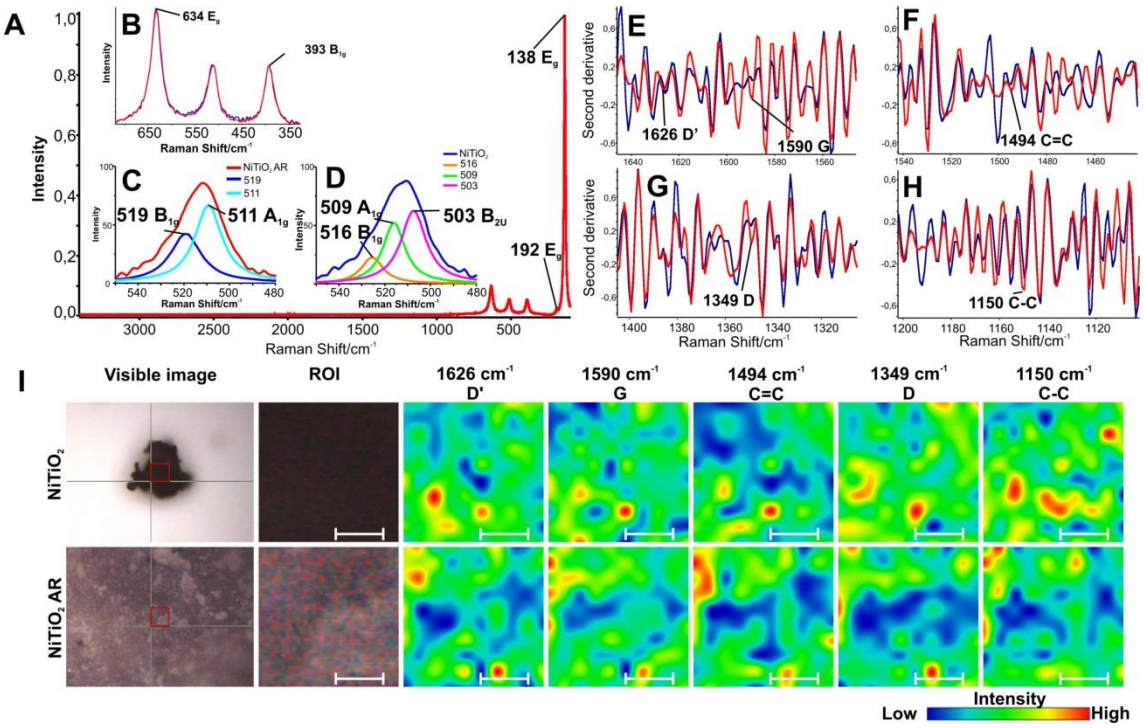

Figure S4. Raman spectra and chemical maps of $NiTiO_2$ before and after reaction (AR). The red spectrum corresponds to the AR sample; the blue spectrum corresponds to the sample before reaction. A) Normalized spectra B) Zoom at the region 720–330 cm^{-1} of the normalized spectra C) Deconvoluted band at ~512 cm^{-1} of the after reaction sample D) Deconvoluted band at ~512 cm^{-1} of the before reaction sample E) Second derivative spectra of the region 1646-1546 cm^{-1} F) Second derivative spectra of the region 1542–1442 cm^{-1} G) Second derivative spectra of the region 1405–1305 cm^{-1} H) Second derivative spectra of the region 1202–1102 cm^{-1} I) Raman maps with distribution of selected bands for $NiTiO_2$ and $NiSiO_2$ AR. The white scale bar corresponds to 4,5 µm.

The single normalized spectra do not reveal significant differences between the sample before and after reaction. Several TiO_2 phonon modes were detected in the spectra: E_g at 138, 192 and 634 cm^{-1} and B_{1g} at 393 cm^{-1} (Fig.S4. A and B). [2] When the second derivative of the spectra was used, major changes in the sample structure occurred. Moreover second derivative spectra of the band at ~512 cm^{-1} showed several TiO_2 phonon modes (two modes in the sample after reaction and three in the sample before reaction). The band was therefore deconvoluted into bands at 503 cm^{-1} - corresponding to B_{2U} mode; 509 cm^{-1} - corresponding to A_{1g} mode; and 516 cm^{-1} - corresponding to B_{1g} in the before reaction sample (Fig.S4. D). In the AR sample deconvolution revealed bands at 511 cm^{-1}, and 519 cm^{-1} corresponding to the A_{1g} and B_{1g} modes, respectively [1] (Fig.S4. C). It shows only slight changes in TiO_2 structure during the reaction, indicating good catalyst stability.

The second derivative spectra (Fig.S4 E, F, G, H) show that after reaction two bands appeared – G band at 1590 cm^{-1} and D band at 1349 cm^{-1} corresponding to highly

crystalline and disordered graphite. D' band at 1626 cm^{-1}, the band corresponding to C=C stretching vibration at 1494 cm^{-1}, and the band corresponding to C-C stretching vibration at 1150 cm^{-1} did not differ among the samples.

There are no significant differences between the spectra—the same peaks may be detected in both before and AR spectra for Fig.S4-6. The spectra differ mainly in the peak height.

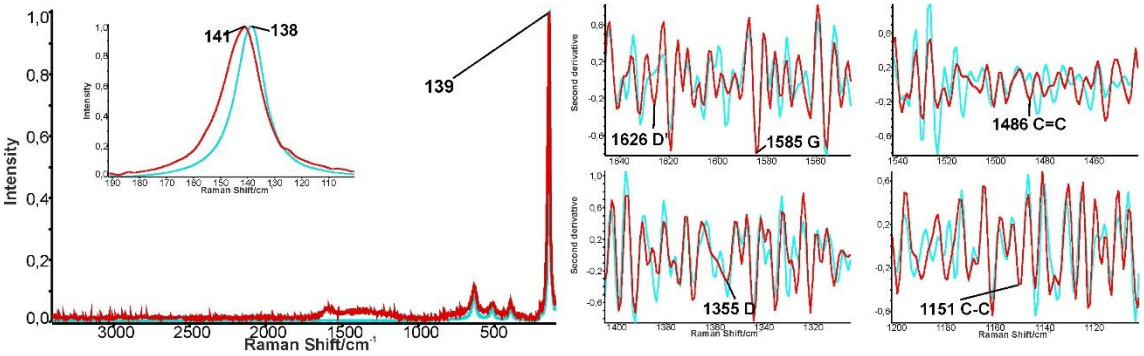

Figure S5. Raman spectra and chemical maps of the $NiVTiO_2$ sample before and after reaction (AR). The red spectrum corresponds to the sample after reaction; the blue spectrum corresponds to the sample before reaction. A) Normalized spectra have the highest band, B) Second derivative spectra of the region 1646–1546 cm^{-1} C) Second derivative spectra of the region 1542–1442 cm^{-1} D) Second derivative spectra of the region 1405-1305 cm^{-1} E) Second derivative spectra of the region 1202–1102 cm^{-1}.

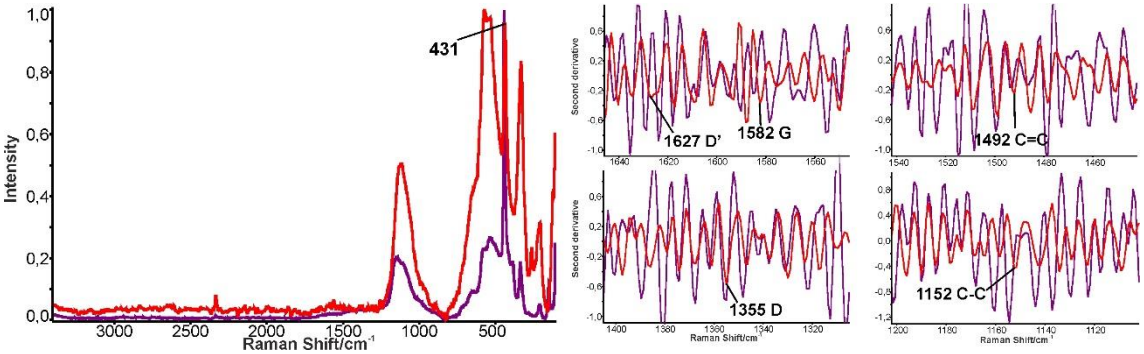

Figure S6. Raman spectra and chemical maps of the NiZnO before and after reaction (AR). The Red spectrum corresponds to the sample after reaction; the blue spectrum corresponds to the sample before reaction. A) Normalized spectra be the highest band, B) Second derivative spectra of the region 1646–1546 cm^{-1} C) Second derivative spectra of the region 1542–1442 cm^{-1} D) Second derivative spectra of the region 1405–1305 cm^{-1} E) Second derivative spectra of the region 1202–1102 cm^{-1}.

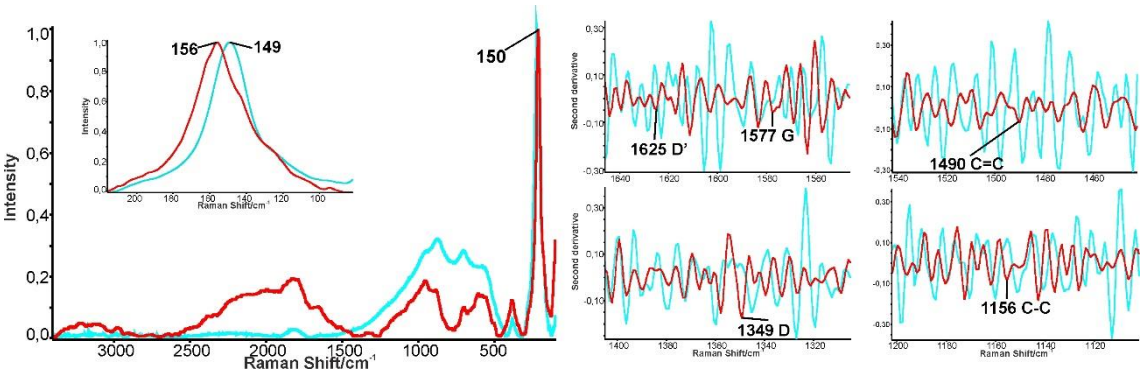

Figure S7. Raman spectra and chemical maps of the Ni/TiSi sample before and after reaction (AR). The red spectrum corresponds to the sample after reaction; the blue spectrum corresponds to the sample before reaction. A) Normalized spectra have the highest band, B) Second derivative spectra of the region 1646–1546 cm^{-1} C) Second derivative spectra of the region 1542–1442 cm^{-1} D) Second derivative spectra of the region 1405–1305 cm^{-1} E) Second derivative spectra of the region 1202–1102 cm^{-1}.